Applied Catalysis A: General 486 (2014) 266–275

Contents lists available at ScienceDirect

Applied Catalysis A: General

journal homepage: www.elsevier.com/locate/apcata

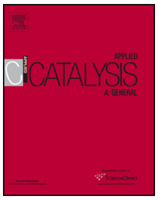

The role of external acid sites of ZSM-5 in deactivation of hybrid CuZnAl/ZSM-5 catalyst for direct dimethyl ether synthesis from syngas

V.V. Ordomsky[a,*], M. Cai[a], V. Sushkevich[b], S. Moldovan[c], O. Ersen[c], C. Lancelot[a], V. Valtchev[d], A.Y. Khodakov[a,**]

[a] Unité de catalyse et de chimie du solide (UMR 8181 CNRS), Université Lille 1-ENSCL-EC Lille, Bat. C3, Cité Scientifique, 59655 Villeneuve d'Ascq, France
[b] Department of Chemistry, Lomonosov Moscow State University, Leninskye Gory 1/3, 119991 Moscow, Russia
[c] Department of Surfaces and Interfaces (DSI), 23, rue du Loess BP 43, F-67034 Strasbourg, France
[d] Laboratoire Catalyse & Spectrochimie, ENSICAEN, 6 Boulevard Maréchal Juin, 14000 Caen, France

ARTICLE INFO

Article history:
Received 18 May 2014
Received in revised form 20 August 2014
Accepted 25 August 2014
Available online 2 September 2014

Keywords:
DME synthesis
Syngas
Deactivation
Cu–ZnO–Al_2O_3
Silylation
ZSM-5

ABSTRACT

Direct synthesis of dimethyl ether (DME) from syngas was investigated on a series of hybrid Cu–ZnO–Al_2O_3/ZSM-5 catalysts prepared by kneading. It was found that the initial performance of the catalysts was a function of both zeolite crystallite sizes and Si/Al ratio. The activity of the hybrid catalysts gradually decreased with time on stream because of simultaneous copper sintering, copper oxidation and ion exchange with zeolite hydroxyl groups. Copper sintering led to the decrease in the number of metal active sites, while ion exchange of Cu^{2+} ions with the hydroxyl groups of the zeolite resulted in lower concentration of acid sites for methanol dehydration. Copper sintering and ion exchange could be slowed down by selective neutralization of the acid sites on the zeolite outer surface by silylation. Both catalyst stability and dimethyl ether productivity were significantly improved.

1. Introduction

Alternative energy sources have recently attracted increasing attention with the raise of environmental concerns and higher crude oil price, which is a consequence of larger worldwide consumption and limited fossil resources [1]. Dimethyl ether (DME) has been considered as a clean alternative diesel fuel because of high cetane number, low auto-ignition temperature and reduced emission of contaminants [2]. Moreover, DME is also an important chemical intermediate for the production of many useful chemicals, such as methyl sulfate, methyl acetate (a precursor to acetic acid), light olefins and BTX aromatics [3,4].

DME can be manufactured from syngas using either two-steps or direct single-step processes. The traditional technology involves two-steps synthesis: the first step is methanol synthesis from syngas on Cu-ZnO-based catalysts ($CO + 2H_2 = CH_3OH$) and the second step is methanol dehydration over acid catalyst such as zeolites and alumina to produce DME ($2CH_3OH = CH_3\text{-}O\text{-}CH_3 + H_2O$). In direct DME synthesis (also named Syngas-to-DME (STD)), carbon monoxide conversion occurs over a bifunctional catalyst in a single reactor. The bifunctional catalyst for direct DME synthesis should combine a methanol synthesis catalyst and a methanol dehydration catalyst. In the two-step DME synthesis, the maximum syngas conversion to methanol is limited by thermodynamics [5], especially at high temperatures. Direct DME synthesis overcomes these thermodynamic constraints. Consequently, a much higher per-pass CO conversion and higher DME productivity could be obtained [6]. Catalyst development for STD reaction has been a subject of a number of publications [7–10].

Copper metal nanoparticles associated with a promoter, i.e. Zn, are usually considered as active phase for methanol synthesis [11]. The advantages of the Cu/Zn system include low cost and high selectivity to methanol. Since methanol synthesis over the Cu–ZnO–Al_2O_3 catalyst is a well-established and optimized technology [12,13], most of the researchers use this catalyst prepared by co-precipitation as one of the components of bifunctional DME synthesis catalyst.

Methanol dehydration to DME requires an acid catalyst [14]. It appears that the acid properties of the dehydration component could play a major role and often affect the overall reaction

---

* Corresponding author. Tel.: +33 320436953
** Corresponding author.
E-mail addresses: vitaly.ordomsky@univ-lille1.fr (V.V. Ordomsky), andrei.khodakov@univ-lille1.fr (A.Y. Khodakov).

http://dx.doi.org/10.1016/j.apcata.2014.08.030
0926-860X/© 2014 Elsevier B.V. All rights reserved.

rate, DME selectivity and catalyst stability. Zeolite based catalysts have several advantages for methanol dehydration to DME relative to more conventional alumina catalysts. The alumina-based catalysts, either pure or doped, are relatively sensitive to steam especially at higher temperatures. A solid acid zeolite-type catalyst, such as HZSM-5 with controlled acidic character exhibits a much higher resistance to steam than alumina [15]. However, the slow diffusion of DME through the zeolite crystals could lead to secondary reactions and formation of undesirable by-products and carbonaceous residues. The latter induces plugging of the catalyst's pores, progressive deactivation and thus demands more frequent catalyst regeneration. Zeolites like ZSM-5 [16,14,17], FER [18], Y [19], MCM-22 [20] are currently the preferred acidic catalysts for the preparation of hybrid catalyst for DME synthesis due to their high acidity and thermal stability.

In order to obtain a good synergy between CO hydrogenation and dehydration of methanol, methanol synthesis and methanol dehydration active phases should be in the close proximity to each other. However, conventional methods which provide the highest degree of mixing between active sites in the composites like impregnation and co-precipitation could be not very efficient in this case. This drawback is a consequence of the interaction of metallic copper with acid sites previously observed in CuO-ZnO/γ-Al_2O_3 [21,6,22] and CuZnAl/SiO_2-Al_2O_3 [23] composites. That was the reason why the most efficient catalysts for DME synthesis reported so far, were prepared using physical mixing of the individual compounds. Recently Tsubaki et al. [24,25] has developed an original technique which can weaken the interaction between methanol synthesis catalyst and zeolite and thus, improve the reaction selectivity to DME. It has been shown [24,25] that core–shell catalyst with Cr/ZnO core and zeolite shell improves DME selectivity by suppressing side reaction such as undesirable hydrocarbon synthesis; C_2–C_4 alkanes are mostly produced.

However, even in the case of the physical mixing or encapsulation method, the interactions of the metals with acid sites could lead to partial deactivation. Several possible reasons of the DME synthesis catalyst deactivation have been reported in the literature: coke deposition [26,27], Cu sintering [28] or copper and zinc ion exchange with protons of zeolite [15,29]. García-Trenco et al. [29] showed the presence of isolated Cu^{2+} cations occupying exchange positions in the HZSM-5 zeolite by EPR spectroscopy. The decrease in Brönsted acidity resulted in suppression of the catalyst activity due to the reduced zeolite activity in methanol dehydration. The same authors studied the influence of zeolite morphology in hybrid CuZnAl/zeolite catalysts in DME synthesis [30]. It was found that the deactivation increased with increasing the external surface area and surface Al concentration of the zeolite co-catalyst. These results confirm that the interactions between metals and acid sites are detrimental for the process since they cause the deactivation of the catalyst during DME synthesis. They also indicate important role of zeolite outer surface area in the deactivation of DME synthesis catalysts. Despite noticeable deactivation of composite CuZnAl/ZSM-5 catalysts in DME synthesis, very few works have addressed so far possible strategies to enhance the catalyst stability. A stable catalyst is indispensable however for the design of efficient processes for direct DME synthesis.

In this work, we have investigated influence of Si/Al ratio, zeolite crystallite size and acid sites on the zeolite outer surface on the structure, catalytic performance and stability of composite Cu–ZnO–Al_2O_3/ZSM-5 catalysts for DME synthesis. A new method is proposed to improve the stability of DME synthesis catalysts.

2. Experimental

2.1. Catalyst preparation

The chemicals used for the catalyst preparation are $Cu(NO_3)_2{\cdot}3H_2O$ (98%, Sigma–Aldrich), $Zn(NO_3)_2{\cdot}6H_2O$ (98%, Sigma–Aldrich), $Al(NO_3)_3{\cdot}9H_2O$ (98.5%, Sigma–Aldrich), Na_2CO_3 (99%, Janssen Chimica), TEOS (98%, Sigma–Aldrich) and hexane (99%, SDS).

The CuO–ZnO–Al_2O_3 catalyst precursor (Cu:Zn:Al = 60:30:10 atomic ratio with the ratio Cu/Zn = 2 and Zn/Al = 3) was prepared by co-precipitation at constant pH (ca. 7) and constant temperature (70 °C). A solution containing metal nitrates ($[Cu^{2+}] + [Zn^{2+}] + [Al^{3+}] = 1.0$ M) and a sodium carbonate solution (1.0 M) were simultaneously added to the reaction vessel containing 10 cm^3 of deionized water. The suspension was continuously stirred and kept at the desired pH by adjustment of the relative flow rates of the two solutions. The final suspension was aged under stirring at 70 °C for 1 h. The precipitate was filtered off, repeatedly washed with sufficient amounts of deionized water to remove residual sodium ions, dried at 110 °C overnight and then finally calcined at 350 °C in flowing air for 6 h yielding the CuO–ZnO–Al_2O_3 catalyst (abbreviated as CZA). The catalytic performance of CZA catalyst in methanol synthesis was found in agreement with previous reports [31].

Three parent ZSM-5 zeolites with different crystallite sizes and Si/Al ratios were used in this work. ZSM-5-I(13) and ZSM-5-I(25) zeolites with Si/Al ratio 13 and 25, respectively, were purchased from Zeolyst. The ZSM-5-II(45) sample with Si/Al ratio of 45 was kindly offered by Süd-Chemie. The aluminum content in the zeolites was determined by ICP analysis. The samples were converted from NH_4 into H-form by calcination in air at 550 °C for 6 h. The surface modified, silylated samples were prepared by the chemical liquid deposition using TEOS as a silica source. 5 g of dried zeolite in H-form was added to the solution of 1 g of TEOS in 50 cm^3 of n-hexane and refluxed for 24 h at 50 °C. The modified sample was dried at 100 °C for 12 h and calcined at 550 °C (heating rate: 2 °C/min) for 5 h in air. The calcined silylated zeolites are denoted as SiO_2/ZSM-5-I(13) and SiO_2/ZSM-5-II(45).

The hybrid catalysts were prepared according to the following procedure. The mixed CZA catalyst with ZSM-5 zeolite was prepared by kneading of the mixture of powders in an agate mortar at a mass ratio of 5:3 (w/w) to form homogeneous hybrid catalyst, followed by pressuring the mixture into tablets and crushing them to 90–150 mesh size particles before the reaction.

2.2. Characterization

The BET surface area, pore volume and average pore diameter were determined by N_2 physisorption using a Micromeritics ASAP 2000 automated system. Each sample was degassed under vacuum at <10 μmHg in the Micromeritics ASAP 2000 at 300 °C for 4 h prior to N_2 physisorption.

NH_3-TPD profiles were obtained in an Autochem 2910 equipment (Micromeritics) coupled with a quadrupole mass spectrometer (OmniStar from Balzers Instruments). Prior to ammonia adsorption, ca. 100 mg of sample was pretreated at 500 °C for 60 min in He. Subsequently, calibrated pulses of NH_3 were introduced at 50 °C until saturation of the sample. The chemisorbed ammonia was then desorbed by heating from 50 to 1000 °C at a heating rate of 10 °C/min. The $m/z = 16$ signal in the coupled mass spectrometer was used to obtain the corresponding NH_3 desorption profiles.

IR spectra were recorded with a Nicolet Protégé 460 FT-IR spectrometer at 4 cm^{-1} optical resolution. Prior to the measurements, the catalysts were pressed in self-supporting discs and activated in the IR cell attached to a vacuum line at 300 °C for 4 h. After activation the samples were reduced in situ with pure hydrogen at 300 °C with subsequent evacuation of the formed water at the same temperature. Adsorption of CO was carried out in the low-temperature cell at −173 °C. Adsorption of pyridine (Py) was performed at 150 °C for 30 min. The excess of Py was further evacuated at 150 °C for 1 h. All spectra were normalized by the weight of the pellet.

Scanning electron microscopy (SEM, Philips XL 30 ESEM-FEG) was used to explore the morphology and size of zeolite crystals.

The TEM analyses were carried out on a Jeol 2100F (field emission gun) microscope operating at 200 kV equipped with a probe corrector for the spherical aberrations. The point-to-point resolution reached was on the order of 2 Å under the parallel TEM mode and 1 Å under the STEM mode. For a better chemical resolution, the micrographs were also acquired in the HAADF mode by using a spot size of 1.1 Å with a current density of 0.5 pA $Å^{-1}$. The energy X-ray dispersive spectroscopic analyses have been performed by using a Li-Si EDS detector with an energy resolution of 0.03 eV. Prior to the analysis, the sample was dispersed by ultrasound in ethanol solution for 5 min, and a drop of solution was deposited onto a carbon membrane onto a 300 mesh-copper grid.

Temperature programmed oxidation (TPO) was used to characterize and quantify the deposited coke on spent catalysts. TPO were performed as follows. 50 mg of catalyst were placed in a plug flow reactor. The catalyst was first pretreated in He at 150 °C for 120 min with subsequent temperature increase to 800 °C with the ramp of 10 °C/min in a He/O_2 (10% O_2) flow of 50 cm^3/min. CO_2 ($m/e = 44$) profiles were recorded using a Varian Saturn III mass spectrometer.

2.3. Catalytic tests

The DME synthesis reaction was carried out in a fixed-bed stainless-steel tubular reactor ($d_{int} = 8$ mm) operating at 20 bar. The catalyst loading was typically 0.5 g. Before reaction, the samples were reduced in hydrogen flow with the flow rate of 30 cm^3/min. During the reduction, the temperature was increased to 290 °C with a ramping rate of 2 °C/min and then kept at this temperature for 7 h. After reduction, the hydrogen flow was switched to a syngas mixture with H_2/CO molar ratio of 2. The reaction was carried out at 260 °C under a pressure of 20 bar maintained using a back pressure regulator, and the space velocity of 3600 $cm^3_{gas}/g^{-1}_{cat}\,h^{-1}$ (WHSV = 1.7 h^{-1}). Carbon monoxide contained 5% nitrogen, which was used as an internal standard for conversion and selectivity calculations. The products were sampled from the high pressure side and analyzed using an online gas chromatograph with a TCD (N_2, CO, CO_2 and CH_4) and a FID (MeOH, DME and hydrocarbons) detectors.

The CO conversion (X) was calculated based on the molar flow rate of CO in the feed ($F_{CO,in}$) and in the outlet streams ($F_{CO,out}$): X_{CO} (%) = $(1-(F_{CO,out}/F_{CO,in}))\times 100$. The product selectivity was determined on carbon basis and expressed in mol% of carbon converted to a specific reaction product.

3. Results and discussion

3.1. Zeolite characterization

The parent zeolite samples had different chemical compositions and also different size and morphology of zeolite crystallites. ZSM-5-I(13) and ZSM-5-I(25) zeolites have uniform particle size distribution in the range 5–7 μm (Figure S1). The zeolite particles consisted of agglomerates of intergrown zeolite crystallites. Again the zeolite crystallites built the agglomerates of sample ZSM-5-II(45), however in this case the individual crystallites with the size ranging between 40 and 100 nm were clearly observed (Figure S1).

Different crystallite sizes of ZSM-5-I(13) and ZSM-5-II(45) result in different low temperature nitrogen adsorption data (Figure S2). The adsorption equilibrium isotherm for ZSM-5-I(13) is of type I in the Brunauer classification and characteristic of microporous solids. The isotherm of ZSM-5-II(45) exhibits an additional step at $p/p_0 \approx 0.8$. The adsorption step in the range of $p/p_0 = 0.8–1.0$ can be explained by filling the intercrystalline pores between nanocrystallites [32].

The ZSM-5-I(13) and ZSM-5-II(45) samples were silylated by TEOS. The kinetic diameter of TEOS (8.9 Å) is much larger than the pore mouth of MFI-type zeolite (5.4–5.6 Å). Thus, only hydroxyl groups on the outer surface could react with hydrolyzed silicon species and form Si—O—Si or Si—O—Al bonds. The analysis of the Al content shows only slight changes in the Si/Al ratio after silylation procedure (Table 1). Previously, silylation with TEOS was used to reduce the concentration of acid sites on the external surface of zeolites [33]. Besides blocking surface activity of zeolite, TEOS and silica species deposited on the external surface might block the zeolite pores and impose diffusion limitations [34]. Low temperature nitrogen adsorption (Table 1 and Figure S2) shows only slight decrease in the total surface area or micropore volume of zeolite ZSM-5-II(45). Differently to ZSM-5-II(45), the silylated ZSM-5-I(13) sample demonstrates a significant decrease in the surface area (from 432 to 350 m^2/g) and volume (from 0.17 to 0.14 cm^3/g). Larger crystallite size and higher acidity of ZSM-5-I(13) result in the higher probability of the pore blockage and decrease in the surface area and volume during silylation in comparison with ZSM-5-II(45).

The acidity of materials was studied by NH_3-TPD (Figure S3, Table 1). All zeolites exhibit a low-temperature (100–300 °C) and a high-temperature (400–600 °C) ammonia desorption peaks. The high temperature peak is usually assigned to ammonia desorption from bridging hydroxyl groups of zeolites (Si-OH-Al) [35]. The identification of the low temperature peak is still controversial. This peak is usually assigned to desorption of physically adsorbed ammonia or desorption of ammonia from silanol groups or extra framework aluminum species [35]. The total amount of acid sites in ZSM-5-I(13) zeolite is almost three times more significant than in ZSM-5-II(45) zeolite. The acidity of ZSM-5 zeolite is usually associated with aluminum content. Thus, higher concentration of acidic sites in the ZSM-5-I(13) zeolite corresponds to higher aluminum content in this zeolite (Table 1). NH_3-TPD shows that silica deposition over ZSM-5-I(13) and ZSM-5-II(45) leads respectively to 6 and 16% decrease in the amount of acid sites in comparison with the parent zeolites, while the strength of acid sites is not affected (Figure

Table 1
Zeolite characterization.

Catalyst	Crystallite size	Si/Al ratio	Al content (mmol/g)	S (m^2/g)	V_{mic} (cm^3/g)	$V_{tot(<350nm)}$ (cm^3/g)	TPD (NH_3) (μmol/g)
ZSM-5-I(13)	5–7 μm	13	1.28	432	0.17	0.23	993
SiO_2/ZSM-5-I(13)	–	14	1.18	350	0.14	0.22	931
ZSM-5-I(25)	5–7 μm	25	0.66	–	–	–	–
ZSM-5-II(45)	40–100 nm	45	0.37	383	0.16	0.63	360
SiO_2/ZSM-5-II(45)	–	48	0.34	354	0.15	0.56	303

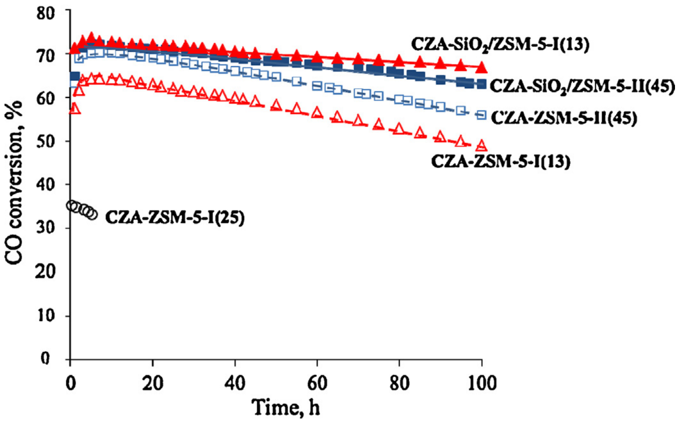

Fig. 1. CO conversion in time during DME synthesis over hybrid catalysts. CZA-zeolite with zeolites before (ZSM-5-I(13), ZSM-5-I(25), ZSM-5-II(45)) and after silylation (SiO_2/ZSM-5-I(13), SiO_2/ZSM-5-I(45)) ($T = 260\,^{\circ}C$, $3600\ cm^3_{gas}/g^{-1}_{cat}\ h^{-1}$, $H_2/CO = 2$, 20 bar).

S3, Table 1). The larger decrease in the amount of acid sites in the ZSM-5-II(45) sample is obviously due to the higher outer surface area of zeolite nanocrystals. A relatively small drop in the concentration of acid sites after silylation confirms preferential adsorption of TEOS on the zeolite outer surface. The ZSM-5 structure is constituted by two intersecting channel systems. Partial blockage of the pores does not affect the total zeolite acidity measured by NH_3-TPD because of relatively small size of NH_3 molecules and their possible migration thought the ZSM-5 channel system.

3.2. Influence of Si/Al ratio and zeolite crystallite size on the catalytic performance of CZA-ZSM-5 catalysts

The catalytic activities and selectivities in DME synthesis of the CZA-zeolite mixture are shown in Figs. 1–3. The carbon monoxide conversions and selectivities are strongly affected by the concentration of acid sites and zeolite crystallite sizes. Note that ZSM-5-I(25) and ZSM-5-I(13) have rather similar morphology and relatively large crystallite sizes (5–7 μm). The strength of acid sites determined by TPD of NH_3 for all zeolites is similar (Figure S3). This suggests that the catalysts principally differ in the concentration of acid sites and in the size of the crystals.

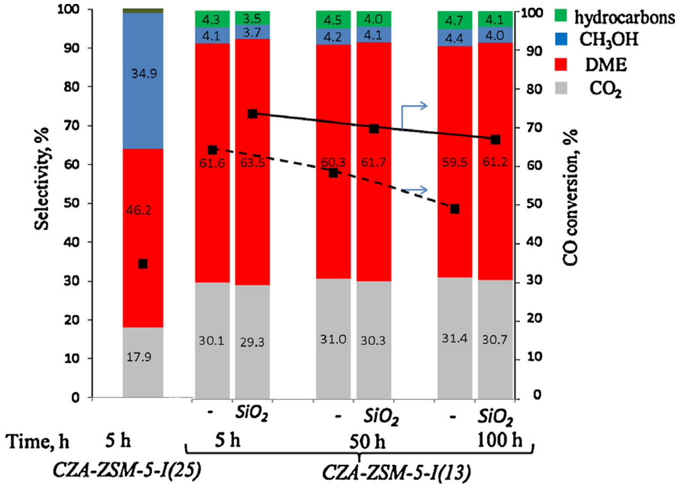

Fig. 2. Selectivity to main products during DME synthesis over CZA hybrid catalyst with ZSM-5-I(25) (TOS 5 h) and with ZSM-5-I(13) before and after silylation (TOS: 5, 50 and 100 h) ($T = 260\,^{\circ}C$, $3600\ cm^3_{gas}/g^{-1}_{cat}\ h^{-1}$, $H_2/CO = 2$, 20 bar).

Let us first evaluate the phenomena due to the different concentration of Brönsted acid sites. The ZSM-5-I(25) zeolite has a concentration of Brönsted acid sites twice lower than ZSM-5-I(13), while the crystallite size is the same for both the zeolites. Interestingly, the activity of the CZA-ZSM-5-I(25) catalyst is much lower compared to the ZSM-5-I(13) counterpart (Fig. 1). Carbon monoxide conversion is about 35% on CZA-ZSM-5(25) in comparison with 65% over CZA-ZSM-5-I(13). In addition, differently to CZA-ZSM-5-I(13), CZA-ZSM-5-I(25) exhibits much higher methanol selectivity (Fig. 2). Higher methanol selectivity on CZA-ZSM-5-I(25) indicates relatively slow kinetics of methanol dehydration which can be due to lower concentration of Brönsted acid sites in this catalyst. The same dependence of the activity of the hybrid catalyst in DME synthesis on Si/Al ratio in zeolites has been observed earlier [36]. Lower carbon monoxide conversion observed on CZA-ZSM-5-I(25) could be also due to thermodynamic constrains. Indeed, methanol is one of the major products on this catalyst and the theoretical equilibrium conversion of CO to methanol is only 20–30% at these conditions [5].

Higher concentration of acid sites in zeolite could be favorable for methanol dehydration. Under the same reaction conditions, CZA-ZSM-5-I(13) with a higher fraction of acid sites exhibits a much higher DME selectivity ($S_{DME} = 61\%$) at the conversion of 65%. The methanol selectivity was only 4% on CZA-ZSM-5-I(13).

In addition to the Brönsted acid sites, zeolite crystallite diameter also affects the performance of CZA-ZSM-5 catalysts. Fig. 1 shows that carbon monoxide conversion on the CZA-ZSM-5-II(45) composite catalyst is comparable to that on CZA-ZSM-5-I(13), although, the number of acid sites in CZA-ZSM-5-II(45) is several times lower than CZA-ZSM-5-I(13). This fact is most probably due to the different crystallite size of these two samples (Figure S1). Indeed, the ZSM-5-I(13) zeolite represents intergrown agglomerates of zeolite crystals with size of around 5–7 μm in comparison with the nanocrystals of ZSM-5-II(45) with size of 40–100 nm. Smaller crystallite sizes of ZSM-5-II(45) should result in higher accessibility of Brönsted sites. This could lead to more efficient methanol dehydration in comparison with ZSM-5-I(13). The higher activity and DME yield during methanol dehydration with decrease in the size of ZSM-5 crystals has been explained earlier by smaller mass transport resistance [37].

The ZSM-5-II(45) based catalyst exhibits DME selectivity of 67% compared to the DME selectivity of 61% observed over CZA-ZSM-5-I(13) at carbon monoxide conversion of 60–70% (Figs. 2 and 3). The ratio of DME to CO_2 selectivities is almost equal to 2:1 over the catalyst containing ZSM-5-I(13). This indicates almost full consumption of water produced in methanol dehydration in WGS reaction. Zeolite could possibly play a role in WGS reaction; the CO_2 selectivity over CZA-ZSM-5-II(45) is significantly lower than on other zeolites. This observation might be attributed to higher concentration of acid sites in ZSM-5-I(13) which should result in the higher water capacity (hold up) in the catalyst. Higher water concentration would result in deeper WGS reaction over this system. The more hydrophobic ZSM-5-II(45) should lead to the lower water adsorption and lower probability of the WGS reaction. In addition CZA-ZSM-5-I(13) produces some amounts of hydrocarbons. The formation of light hydrocarbons over CZA-ZSM-5-I(13) might be explained by higher concentration of acid sites and thus by higher probability of methanol and DME conversion into olefins in comparison with CZA-ZSM-5-II(45). The presence of saturated hydrocarbons (ethane, propane, butane) is probably due to subsequent hydrogenation of olefins into alkanes over CZA [12]. Methane formation is most probably a result of CO and CO_2 hydrogenation over CZA catalyst. Indeed, some amounts of methane are usually observed in syngas conversion on copper catalysts [38]. Hydrocarbon production over CZA-ZSM-5 catalyst could be possibly reduced by selective neutralization of strong zeolite acid sites. Previously it

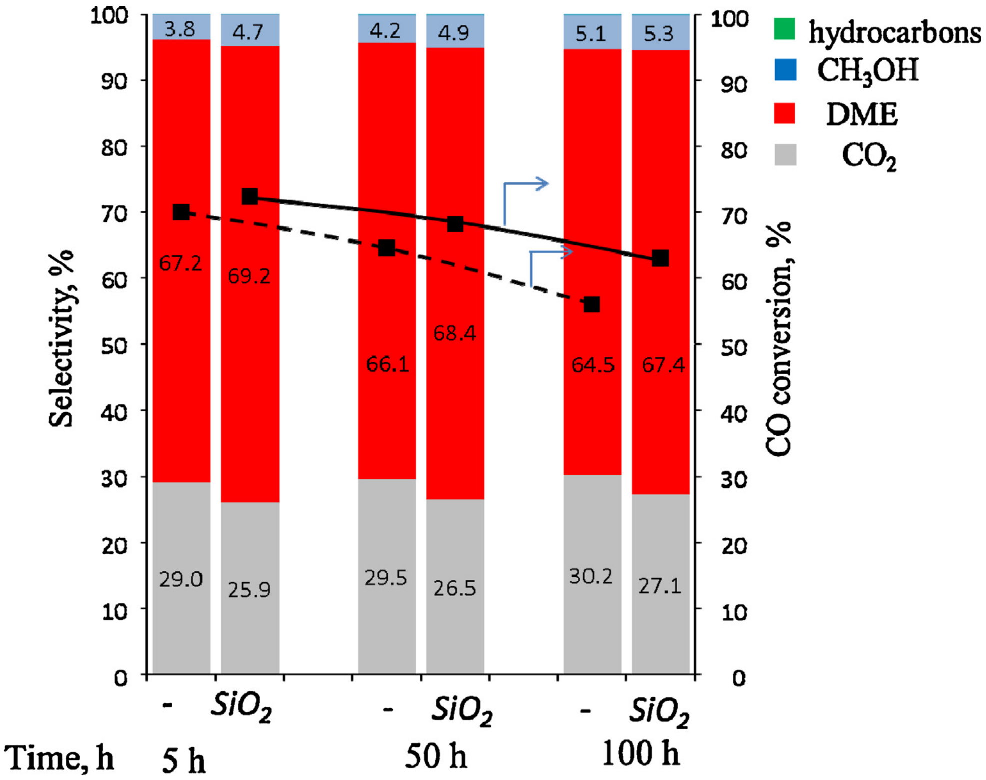

Fig. 3. Selectivity to main products during DME synthesis over CZA hybrid catalyst with ZSM-5-II(45) before and after silylation (TOS: 5, 50 and 100 h) (T = 260 °C, 3600 cm$^3_{gas}$/g$^{-1}_{cat}$ h^{-1}, H$_2$/CO = 2, 20 bar).

was shown that modification of ZSM-5 by Sb$_2$O$_3$ or MgO increased the selectivity to DME from 55 to 65–69% [12,39]. In addition, higher DME selectivity can be also favored by smaller zeolite crystallite sizes. Smaller ZSM-5-II(45) crystallite size reduces methanol and DME residence time inside the zeolite matrix and thus the probability of secondary reactions (e.g. hydrocarbon formation).

3.3. Influence of silylation of zeolite external surface on the catalyst structure and stability

3.3.1. Catalytic properties of catalysts with silylated zeolites

One of the major problems of direct DME synthesis from syngas is catalyst deactivation. All studied CZA-ZSM-5 composite catalysts showed gradual decrease in carbon monoxide conversion with time on stream (Fig. 1). The CO conversion decreased for the CZA-ZSM-5-I(13) catalyst from 64 to 49% and for CZA-ZSM-5-II(45) from 70 to 56% respectively during the first 100 h of the reaction. The results are consistent with previous reports about the stability of CZA-ZSM-5 catalysts prepared by kneading [15].

The stability of CZA-ZSM-5-I(13) and CZA-ZSM-5-II(45) catalysts was improved in this work using silylation with TEOS. Fig. 1 shows that the conversion on both the silylated zeolites was much more stable than on the parent catalysts. For CZA-ZSM-5-I(13) catalyst silylation also led to the increase in initial carbon monoxide conversion from 63 to 74%. Higher DME selectivity was also observed on silylated catalysts. For CZA-ZSM-5-I(13), silylation leads to the increase in DME selectivity from 61 to 63% after 5 h of the reaction, while for CZA-ZSM-5-II(45) the DME selectivity rises after silylation from 67 to 69%. At the same time, the selectivity to CO$_2$ decreases on both catalysts. Lower CO$_2$ selectivity after silylation can be attributed to lower WGS activity over more hydrophobic CZA-ZSM-5-II(45) and might be explained again by a decrease in the concentration of adsorbed water after the interface between CZA catalyst and zeolite after silylation. In order to identify the reasons of deactivation and to evaluate the influence on silylation on the catalyst stability, the parent and silylated hybrid CZA-zeolite catalysts before and after the catalytic experiments have been extensively studied by TEM and FTIR spectroscopy.

3.3.2. Physicochemical properties of catalysts before and after deactivation

Zeolite acidity in the fast deactivating hybrid CZA-ZSM-5-I(13) has been investigated by Py adsorption. Fig. 4 shows the results of Py adsorption over CZA-ZSM-5-I(13) before and after the catalytic tests. In the range of 1400–1700 cm^{-1}, chemically adsorbed pyridine exhibited a usual set of bands: two bands at 1545 and 1656 cm^{-1} assigned to pyridinium ion (PyH$^+$), two bands at 1450

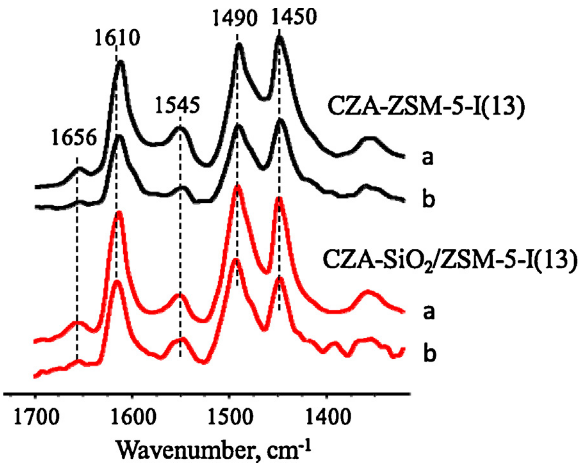

Fig. 4. IR spectra of Py adsorption over the CZA-ZSM-5-I(13) hybrid non silylated catalyst before (a) and after the reaction (b) and over silylated catalyst before (a) and after the reaction (b). The catalysts were (re)-reduced prior to Py adsorption.

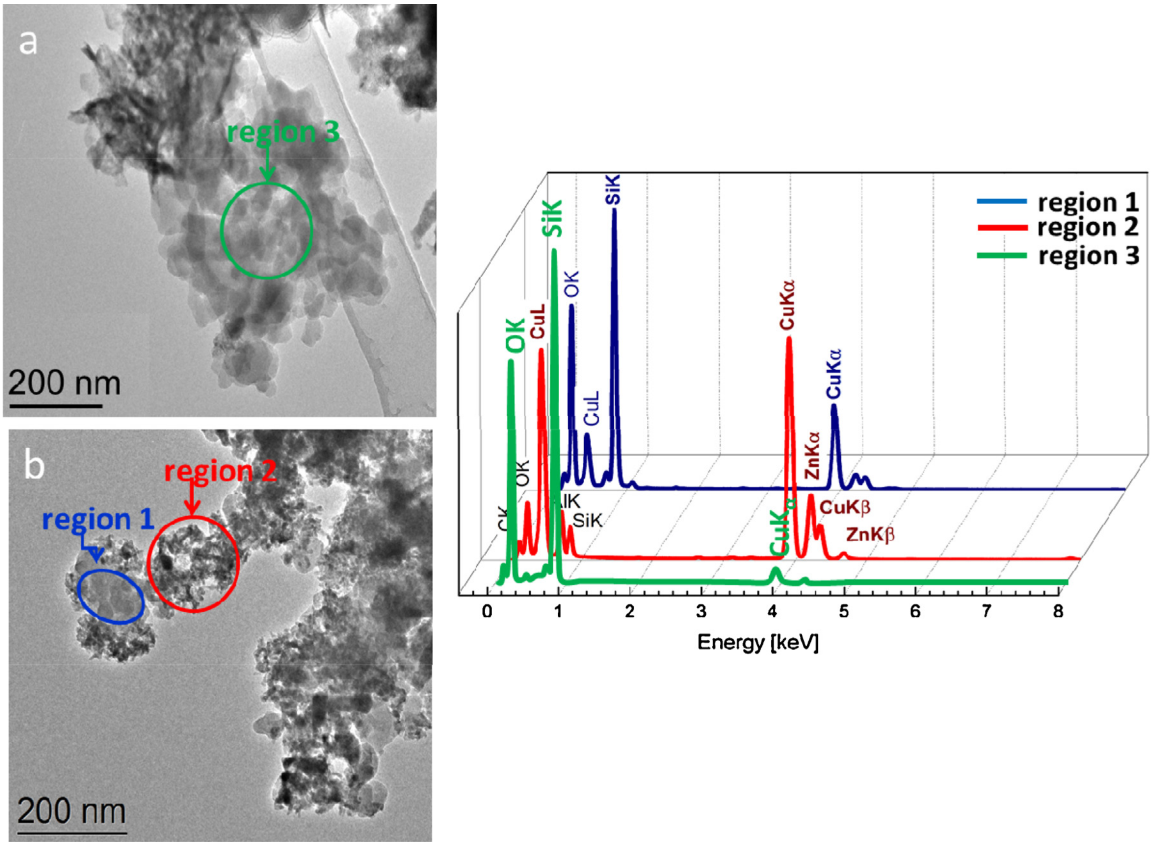

Fig. 5. TEM micrographs and corresponding EDX spectra of a representative region within the CZA-ZSM-5-I(13) catalyst before (a) and after reaction (b). The encircled areas represent a ZSM-5 Si-rich region (blue and green) and Co and Zn-rich area (red) as identified by the EDX analysis. (For interpretation of the references to color in this figure legend, the reader is referred to the web version of this article.)

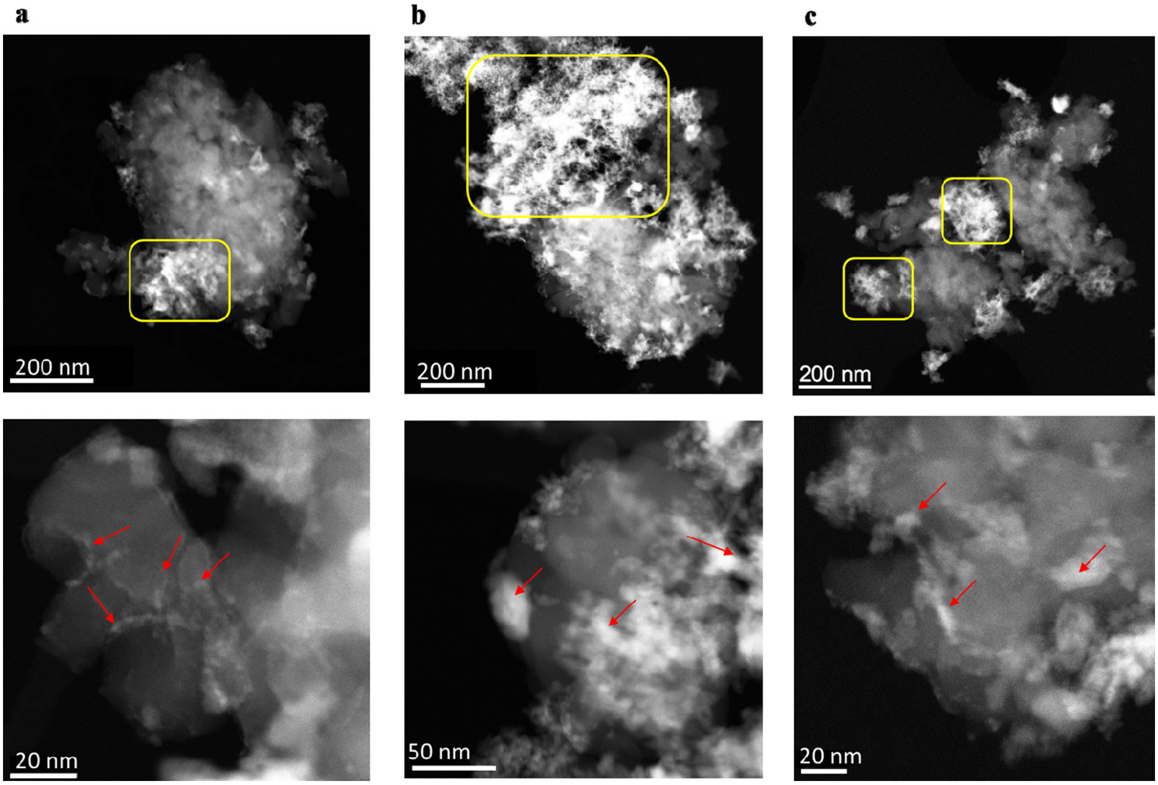

Fig. 6. STEM-HAADF micrographs of the CZA-ZSM-5-I(13) hybrid catalysts before the reaction (a), after the reaction (b) and CZA-SiO$_2$/ZSM-5-I(13) after the reaction (c). The rectangular areas mark the metal-rich regions, whereas the red arrows point to metallic atomic clusters and/or nanoparticles. (For interpretation of the references to color in this figure legend, the reader is referred to the web version of this article.)

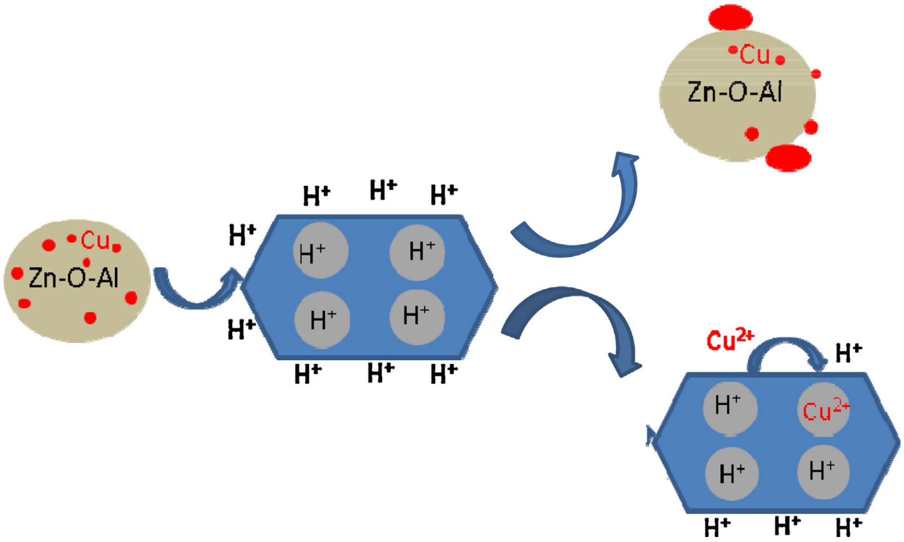

Fig. 7. Schematic presentation of copper migration leading simultaneously to ion exchange with hydroxyl groups of the ZSM-5 zeolite and copper sintering.

and 1610 cm^{-1} related to coordinatively adsorbed pyridine on Lewis sites. The band at 1490 cm^{-1} was attributed to Py species adsorbed on Lewis and Brönsted sites [40]. The intensity of the band corresponding to pyridinium ion (PyH$^+$) significantly decreases after the catalytic experiment. This corresponds to the decrease in the number of Brönsted acid sites. The Lewis acidity remains almost unchanged for both catalysts before and after the reaction. In addition to the zeolite Lewis sites, the Lewis acidity in the spent catalysts seems to be also related to cationic copper species which concentration may increase during the reaction.

In order to find the reasons responsible for the drop in the number of Brönsted acid sites after the reaction, the local elemental composition of hybrid CZA-ZSM-5-I(13) catalyst before and after catalytic experiment was analyzed by TEM-EDX and STEM-HAADF (Fig. 5). Owing to the contrasts in the TEM mode, we were able to distinguish between the zeolite and metal-rich regions. The chemical composition of these regions was further investigated using EDX. Silicon was predominant in the zeolite area of the catalysts before and after reaction as shown by Fig. 5 (blue and green encircled region and spectra), whereas the other regions, which show different contrasts, appear to be dominated by Cu, Zn and at smaller expense Al. The mean size of the zeolite crystals is of several tens of nm, whereas the CZA grains appear as platelets (ZnO) or needle-like shaped (alumina) with mean sizes of about 20 nm. Catalyst spacemen were deposited on a carbon membrane supported by a Cu grid. Consequently, traces of Cu (region 1) could be detected in regions that appear to be pure zeolite. Note however, that the signal of Cu from the catalyst before reaction (region 3) was significantly lower in comparison with the signal from the region 1 indicating the presence of Cu within the zeolite crystal or in the close proximity to zeolite crystal after the reaction. Taking into account the decrease in the number of Brönsted acid sites in zeolite, this observation might be explained by migration of copper during the reaction followed by ion exchange of copper ions with zeolite hydroxyl groups. Similar phenomenon was observed earlier by the group of Martínez [29] at higher temperatures with identification of Cu^{2+} by EPR. The authors suggested that interaction between protons and Cu is one of the main reasons of the catalyst deactivation [29,30].

The metal distribution within the CZA-ZSM-5 catalysts was studied by direct analysis of contrasts from the STEM-HAADF micrographs. Because of higher sensitivity to the *Z* atomic number, this mode is particularly suitable for the assessment of the distribution of metallic nanoparticles. The metal distribution in CZA-ZSM-5-I(13) zeolite composite with and without the TEOS treatment has been analyzed before and after reaction (Fig. 6). After catalyst activation in hydrogen (Fig. 6a), Cu is located exclusively on the CZA grains, either as NPs with a mean size of 5 nm or as a thin metallic layer. The thickness of the Cu metallic layer varies from several nm to 15 nm, as depicted by Fig. 6a. After the reaction, the morphology of the catalyst changes drastically in terms of metal distribution. Larger metal NPs with mean sizes superior to 10–15 nm are detected not only on the CZA grains but on the zeolite as well (Fig. 6b). The thin metal layer completely disappeared from the grains, most probably being assimilated by the larger neighboring particles during the reaction. This phenomenon can be interpreted by assuming metal sintering on the surface of the CZA and subsequent copper diffusion to the zeolite. Such phenomenon can be responsible for copper migration followed by oxidation, subsequent exchange of Cu^{2+} ions with zeolite hydroxyl groups. The outline of the catalyst deactivation processes is shown in Fig. 7.

The spent silylated CZA-SiO$_2$/ZSM-5-I(13) sample shows major difference in location of copper NPs, relative to the non-silylated catalyst (Fig. 6). The STEM-HAADF analysis shows a clear separation of CZA and zeolite phases in spent CZA-SiO$_2$/ZSM-5-I(13) catalyst. Differently to the spent CZA-ZSM-5-I(13) catalyst prepared without TEOS pretreatment, copper species were not detected in CZA-SiO$_2$/ZSM-5-I(13) inside the zeolite.

Thus, TEM-EDX and STEM-HAADF have provided valuable information on copper localization in the silylated CZA-zeolite prior and after the reaction. Silylation of zeolite surface by TEOS results in less significant Cu sintering and ion exchange with zeolite protons. Consequently, the silylated catalyst shows better stability (Fig. 1). Our results suggest that neutralization of hydroxyl group at the external surface reduces copper sintering and ion exchange with protons of zeolites (Fig. 7) which are usually observed on non-silylated catalysts.

Cu sintering in Cu-ZSM-5 catalyst during NO decomposition was observed previously. Fierro et al. [41] found that migration of Cu inside of zeolite pores was facilitated by the presence of water vapor. Water promotes formation of positively charged mobile copper clusters. Copper sintering seems to proceed according to particle migration and coalescence mechanism. Similar mechanism of nanoparticle sintering facilitated by the presence of water was previously observed for supported nickel and cobalt catalysts [42,43]. In addition to water, hydroxyl groups on the zeolite outer surface can obviously contribute to higher copper mobility

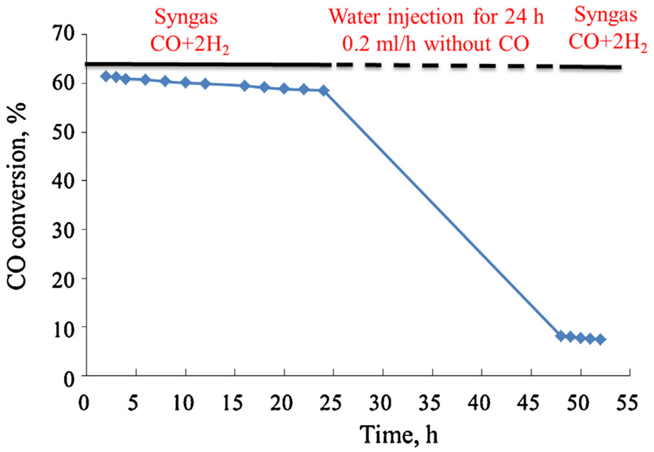

Fig. 8. CO conversion in time during DME synthesis ($T = 260\,^{\circ}C$, 3600 $cm^3_{gas}/g^{-1}_{cat}\,h^{-1}$, $H_2/CO = 2$, 20 bar) over hybrid catalysts CZA-ZSM-5-I(13) before and after addition of 0.2 cm^3/h of H_2O during 24 h in hydrogen flow ($T = 260\,^{\circ}C$, 1200 $cm^3_{H_2}/g^{-1}_{cat}\,h^{-1}$, 20 bar).

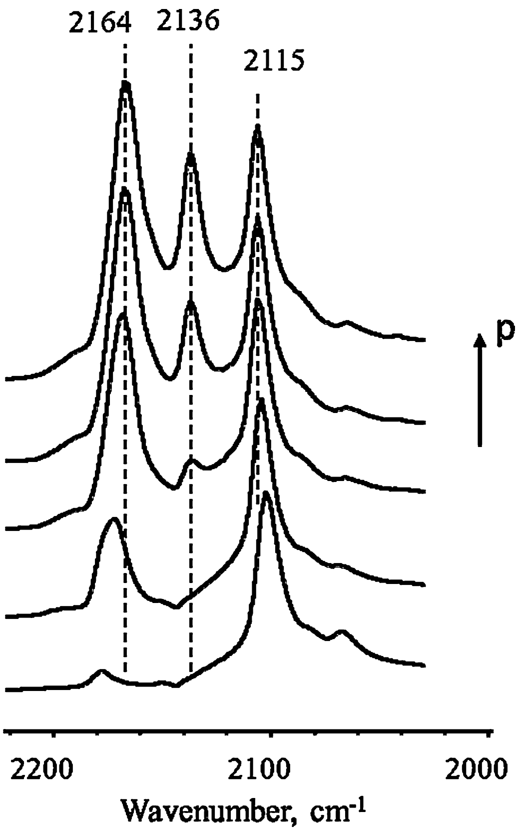

Fig. 9. FTIR spectra of CZA-ZSM-5-I(13) hybrid catalyst after adsorption of CO at low temperature (−173 °C) at gradually increasing pressures. The catalyst was reduced prior to CO adsorption.

in hybrid catalysts. Water seems to play a major role in copper sintering. To identify the effect of water on copper sintering, we conducted a specific experiment. In this experiment, water was added to the catalyst in a flow of hydrogen in the absence of carbon monoxide (Fig. 8). The amount of added water roughly corresponded to water amounts produced under typical reaction conditions (DME synthesis). Fig. 8 shows that the conversion of CO decreases rapidly from 60 to 10% after 24 h of catalyst exposure to water and hydrogen at the reaction temperature. This suggests that indeed water significantly facilitates the migration of Cu.

The changes in the oxidation state during the reaction were also investigated by FTIR spectroscopy using low temperature CO adsorption. Fig. 9 displays IR spectra of CO adsorption as a function of coverage over parent CZA-ZSM-5-I(13). At the very low coverage the most intense band is found at 2115 cm^{-1}. Further addition of CO leads to the appearance of the band at 2170 cm^{-1} which shifts to 2164 cm^{-1} with the increase in the amount of adsorbed CO. Finally another band emerges at 2136 cm^{-1}. The lower frequency band at 2115 cm^{-1} corresponds to the strongest adsorption of CO. In agreement with previous reports [44–46], the band at 2115 cm^{-1} could be related to the reduced copper species (Cu^0 or Cu^+). It is well known that copper carbonyls are not very stable. Copper carbonyl stability could be enhanced when CO adsorbs on well dispersed nanoparticles at low temperature. The band at 2164 cm^{-1} might be assigned to CO adsorption over Brönsted acid sites [47]. The same band might also have CO adsorbed either to extra framework cations (Zn^{2+}, Cu^{2+}). The band at 2136 cm^{-1} is usually assigned to physically adsorbed CO. It appears only at relatively higher carbon monoxide pressures.

Fig. 10 shows IR spectra of adsorbed CO on the pure CZA and hybrid catalysts prepared using the parent and silylated ZSM-5-I(13) zeolites before and after the reaction. The spectrum of CO adsorbed over pure CZA shows bands of CO at 2164 and 2115 cm^{-1}. Mixing of CZA with parent and silylated ZSM-5-I(13) zeolites results in modification of the band shape and intensity. The intensity of the band at 2164 cm^{-1} increases for the non-modified zeolite system and almost does not change in the case of silylated ZSM-5. Taking into account that Brönsted acidity decreases during reaction over CZA-ZSM-5-I(13), the increase in the intensity of the band at 2164 cm^{-1} might be possibly explained by high adsorption of CO over forming cationic Cu^{2+} sites. In the case of silylated sample, the band of CO over metallic Cu is still broad and shifts to higher wavenumbers similarly to parent CZA. It is indicative of the presence of Cu sites with slightly different electronic properties or chemical environment [48]. The position of this band is more affected by the reaction in non silylated ZSM-5-I(13) catalyst. Mixing with parent zeolite results in significant narrowing of the band and a low frequency shift of the band at 2164 cm^{-1}. This fact might be explained by interaction of zeolite [49] with

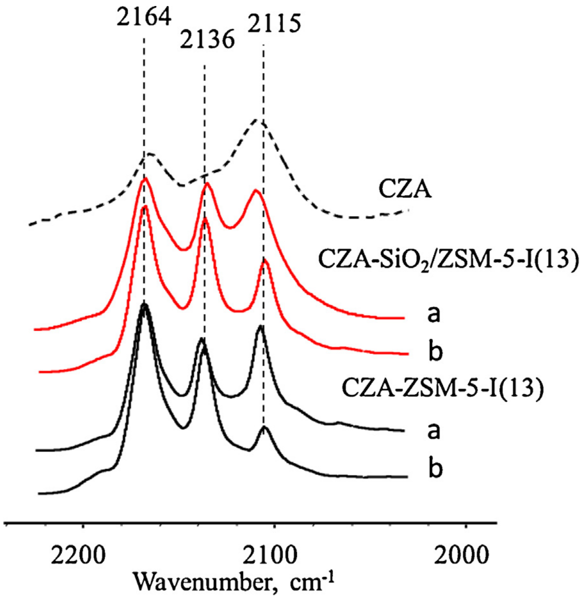

Fig. 10. IR bands resulting from CO adsorption at −173 °C on the CZA catalyst, CZA-ZSM-5-I(13) hybrid catalyst before (a) and after the reaction (b) and on the CZA-SiO_2/ZSM-5-I(13) hybrid catalyst before (a) and after the reaction (b). The catalysts were reduced prior to CO adsorption.

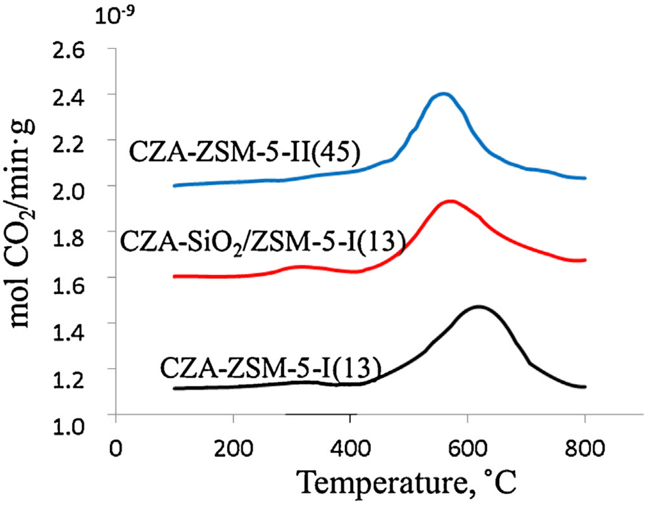

Fig. 11. TPO of the CZA-ZSM-5-I(13), CZA-ZSM-5-II(45) and CZA-SiO_2/ZSM-5-I(13) hybrid catalysts after the reaction with detection of CO_2.

positively charged copper clusters in CZA which may form in the catalyst during the pretreatments. It is interesting to note that the non-silylated catalyst shows a significant decrease in the intensity of the band at 2115 cm^{-1} after the reaction. Low intensity of the band at 2115 cm^{-1} can be assigned to the low concentration of available copper sites in the spent CZA-ZSM-5-I(13) catalyst probably because of copper sintering, oxidation and ion exchange. At the same time, the intensity of the band at 2115 cm^{-1} attributed to copper metal sites in the silylated catalysts is affected to a much lesser extent by the exposure to the reaction conditions. Neutralization of the acid sites on zeolite outer surface seems to prevent copper migration with its ion exchange and sintering in SiO_2/ZSM-5-I(13). Our results correlate with the results of the group of Martínez [30] who observed the effect of the external surface area and surface Al concentration of the zeolite co-catalyst on the catalyst deactivation.

Thus, the pronounced increase in the catalyst stability during DME synthesis after silylation might be explained by suppression of Cu migration and ion exchange on the outer surface of zeolite due to neutralization of the surface acid sites by TEOS. The possible alternative explanation of the catalyst deactivation could be coke formation during reaction. The coke may form by polymerization of olefins or condensation of reactive oxygenates during reaction [26,27]. In order to verify this assumption, TPO of the spent catalysts has been conducted with detection of forming CO_2 (Fig. 11). The results indicate similar character of the adsorbed coke species for all samples. The amount of forming CO_2 is very low ($7–8 \times 10^{-6}$ mmol/g) and comparable for silylated and non silylated ZSM-5-I(13) and ZSM-5-II(45) zeolites. These results suggest that silylation does not influence to any noticeable extent coke deposition. The experiment with addition of water (Fig. 8) also supports this assumption.

Note that silylation can improve not only the catalyst stability but also the catalyst initial activity. One might anticipate that copper on the surface of CZA reacts with the protons of non-silylated ZSM-5-I(13) already during pretreatment of the catalyst in the reactor. It reduces amount of active Cu species for methanol synthesis. Significant interaction between ZSM-5 and CZA with ion exchange of Cu during hybrid catalyst preparation has been observed earlier [29,30]. In the silylated catalyst, the reaction between copper and Brönsted acid sites during activation could be hindered by SiO_2 protective layer on the zeolite outer surface. Thus, the silylated catalyst can show higher reaction rate compared to non-silylated counterpart immediately after the exposure to the reaction medium.

The selectivity slightly evolves with reaction time over both the parent and silylated catalysts. The selectivity to DME decreases by 2–3% over parent catalysts with simultaneous very slight increase in the selectivity to CO_2 and methanol (Figs. 2 and 3). A slight increase in methanol selectivity is related to the continuous decrease in the concentration of Brönsted acid sites during the reaction and thus slower methanol dehydration rate. The acid sites in pores of the parent non-silylated zeolites are neutralized by migrating Cu^{2+} ions. At the same time, these catalysts can show a higher activity in WGS reaction which can be due to easier water dissociation over Cu^{2+} ions [50]. At the same time, silylation of zeolite outer surface hinders copper migration into zeolite pores. Thus, the concentration of zeolite acid sites is reduced to a lesser extent in the silylated samples during the reaction. Silylation leads to the increase in the selectivity to DME by 2% over both catalytic systems. This corresponds to the highest selectivity to DME (69%) observed on SiO_2/ZSM-5-II catalyst [39]. The increase in DME selectivity after silylation is accompanied by a significant decrease in the selectivity to CO_2 and hydrocarbons. Previously it was shown that DME selectivity could be improved by the promotion of copper-zeolite catalysts by metal oxides (ZrO_2, MgO, Sb_2O_3). Indeed, addition of metal oxides reduces zeolite acidity and hydrocarbon production. However promotion with metal oxides does not improve the catalyst stability [12,16,39]. Indeed, metal oxides are usually distributed almost uniformly inside the zeolite lattice. Silylation with TEOS results in selective neutralization of the acid sites on the zeolite surface and produces a much more significant effect on the catalyst stability than the promotion with metal oxides.

4. Conclusion

The catalytic performance of hybrid Cu–ZnO–Al_2O_3/ZSM-5 prepared by kneading in direct DME synthesis from syngas depends on the zeolite crystallite size and Si/Al ratio. Higher concentration of the zeolite Brönsted acid sites and smaller zeolite crystallite sizes favor higher DME productivity.

The decrease in the catalytic performance of hybrid catalysts with time on stream is due to the combination of several phenomena: copper sintering, copper oxidation, migration and ion exchange with hydroxyl groups in zeolite pores.

The catalyst stability can be enhanced by selective neutralization of acid sites on zeolite outer surface with TEOS. Selective neutralization of Brönsted acid sites on the outer zeolite surface slows down copper sintering and migration and results in the better catalyst stability and slightly higher selectivity to DME. The effect of silylation on the catalytic performance and stability was more pronounced for the zeolite with abundant Brönsted acidity and small outer surface area.

Acknowledgments

This research is being performed within the ANR project CATSYN-BIOFUELS (ANR-12-BS07-0029). The authors gratefully acknowledge the support of the French National Research Agency.

Appendix A. Supplementary data

Supplementary data associated with this article can be found, in the online version, at http://dx.doi.org/10.1016/j.apcata.2014.08.030.

References

[1] A. Corma, S. Iborra, A. Velty, Chem. Rev. 107 (2007) 2411–2502.
[2] T.A. Semelsberger, R.L. Borup, H.L. Greene, J. Power Sources 156 (2006) 497–511.

[3] W.W. Kaeding, S.A. Butter, J. Catal. 61 (1980) 155–164.
[4] G. Cai, Z. Liu, R. Shi, C. He, L. Yang, C. Sun, Y. Chang, Appl. Catal. A 125 (1995) 29–38.
[5] L.R. Clausen, B. Elmegaard, J. Ahrenfeldt, U. Henriksen, Energy 36 (2011) 5805–5814.
[6] J.L. Li, X.G. Zhang, T. Inui, Appl. Catal. A 147 (1996) 23–33.
[7] Y. Tan, H. Xie, H. Cui, Y. Han, B. Zhong, Catal. Today 104 (2005) 25–29.
[8] J.W. Jung, Y.J. Lee, J.W. Bae, Appl. Catal. B 126 (2012) 1–8.
[9] G. Yang, N. Tsubaki, J. Shamoto, Y. Yoneyama, J. Am. Chem. Soc. 132 (2010) 8129–8136.
[10] R. Nie, H. Lei, S. Pan, L. Wang, J. Fei, Fuel 96 (2012) 419–425.
[11] H.Y. Chen, S.P. Lau, L. Chen, J. Lin, C.H.A. Huan, K.L. Tan, J.S. Pan, Appl. Surf. Sci. 152 (3) (1999) 193–199.
[12] D. Mao, W. Yang, J. Xia, J. Catal. 230 (2005) 140–149.
[13] J.W. Bae, S.-H. Kang, Y.-J. Lee, K.-W. Jun, Appl. Catal. B 90 (2009) 426–435.
[14] M. Xu, J.H. Lunsford, D.W. Goodman, A. Bhattacharyya, Appl. Catal. A 149 (1997) 289–301.
[15] T. Takeguchi, K. Yanagisawa, T. Inui, M. Inoue, Appl. Catal. 192 (2000) 201–209.
[16] A. García-Trenco, A. Martínez, Appl. Catal. A 411–412 (2012) 170–179.
[17] Q. Zhang, Y. Tan, C. Yang, H. Xie, Y. Han, J. Ind. Eng. Chem. 19 (2013) 975–980.
[18] S.-H. Kang, J.W. Bae, K.-W. Jun, H.S. Potdar, Catal. Commun. 9 (2008) 2035–2039.
[19] D. Jin, B. Zhu, Z. Hou, J. Fei, H. Lou, X. Zheng, Fuel 86 (2007) 2707–2713.
[20] D. Mao, J. Xia, B. Zhang, Q. Chen, G. Lu, Chin. J. Catal. 29 (2008) 945–949.
[21] Q. Ge, Y. Huang, F. Qiu, S. Li, Appl. Catal. A 167 (1998) 23–30.
[22] G.R. Moradi, S. Nosrati, F. Yaripor, Catal. Commun. 8 (2007) 598–606.
[23] S.P. Naik, H. Du, H. Wan, V. Bui, J.D. Miller, W.W. Zmierczak, Ind. Eng. Chem. Res. 47 (2008) 9791–9794.
[24] K. Pinkaew, G. Yang, T. Vitidsant, Y. Jin, C. Zeng, Y. Yoneyama, N. Tsubaki, Fuel 111 (2013) 727–732.
[25] G. Yang, M. Thongkam, T. Vitidsant, Y. Yoneyama, Y. Tan, N. Tsubaki, Catal. Today 171 (1) (2011) 229–235.
[26] J. Abu-Dahrieh, D. Rooney, A. Goguet, Y. Saih, Chem. Eng. J 203 (2012) 201–211.
[27] I. Sierra, J. Erena, A.T. Aguayo, J.M. Arandes, M. Olazar, J. Bilbao, Appl. Catal. B 106 (2011) 167–173.
[28] J.W. Jung, Y.J. Lee, S.H. Um, P.J. Yoo, D.H. Lee, K.-W. Jun, J.W. Bae, Appl. Catal. B 126 (2012) 1–8.
[29] A. García-Trenco, A. Vidal-Moya, A. Martínez, Catal. Today 179 (2012) 43–51.
[30] A. García-Trenco, S. Valencia, A. Martínez, Appl. Catal. A 468 (2013) 102–111.
[31] J. Li, W. Zhang, L. Gao, P. Gu, K. Sha, H. Wa, Appl. Catal. A 165 (1997) 411–417.
[32] A. Simon-Masseron, J.P. Marques, J.M. Lopes, F. Ramoa Ribeiro, I. Gener, M. Guisnet, Appl. Catal. A: Gen. 316 (2007) 75–82.
[33] S.R. Zheng, R.H. Heydenrych, A. Jentys, J. Phys. Chem. B 106 (37) (2002) 9552–9558.
[34] R.W. Weber, K.P. Möller, C.T. O'Connor, Microporous Mesoporous Mater. 35–36 (2000) 533–543.
[35] C.V. Hidalgo, H. Itoh, T. Hattori, M. Niwa, Y. Murakami, J. Catal. 85 (1984) 362–369.
[36] J.-H. Kim, M.J. Park, S.J. Kim, O.-Sh. Joo, K.-D. Jung, Appl. Catal. A 264 (2004) 37–41.
[37] A.A. Rownaghi, F. Rezaei, M. Stante, Appl. Catal. B 119–120 (2012) 56–61.
[38] J. Wang, P.A. Chernavskii, A.Y. Khodakov, Y. Wang, J. Catal. 286 (2012) 51–61.
[39] D. Mao, J. Xia, B. Zhang, G. Lu, Energy Convers. Manage. 51 (2010) 1134–1139.
[40] M. Guisnet, P. Ayrault, C. Coutanceau, M.F. Alvarez, J. Datka, J. Chem. Soc., Faraday Trans. 93 (1997) 1661–1665.
[41] G. Fierro, G. Ferraris, G. Moretti, Appl. Catal. B 91 (2009) 499–506.
[42] J. Sehested, J. Catal. 217 (2003) 417–426.
[43] M. Sadeqzadeh, J. Hong, P. Fongarland, D. Curulla-Ferré, F. Luck, J. Bousquet, D. Schweich, A.Y. Khodakov, Ind. Eng. Chem. Res. 51 (2012) 11955–11964.
[44] A.E. Baber, X. Yang, H. You Kim, K. Mudiyanselage, M. Soldemo, J. Weissenrieder, S.D. Senanayake, A. Al-Mahboob, J.T. Sadowski, J. Evans, J.A. Rodriguez, P. Liu, F.M. Hoffmann, J.G. Chen, D.J. Stacchiola, Angew. Chem. 53 (2014) 5336–5340.
[45] V. Sanchez-Escribano, L. Arrighi, P. Riani, R. Marazza, G. Busca, Langmuir 22 (2006) 9214–9219.
[46] G. Busca, U. Constantino, F. Marmottini, T. Montanari, P. Patrono, F. Pinzari, G. Ramis, Appl. Catal. A 310 (2006) 70–78.
[47] S. Bordiga, E.E. Platero, C.O. Arean, C. Lamberti, A. Zecchina, J. Catal. 137 (1992) 179–185.
[48] A. Kitla, O.V. Safonova, K. Föttinger, Catal. Lett. 143 (2013) 517–530.
[49] G. Morterra, E. Giamello, G. Cerrato, G. Centi, S. Perathoner, J. Catal. 179 (1998) 111–128.
[50] G.G. Olympiou, C.M. Kalamaras, C.D. Zeinalipour-Tazdi, A.M. Efstathiou, Catal. Today 127 (2007) 304–318.